An Improved Framework for Superparameterization

WOJCIECH W. GRABOWSKI

National Center for Atmospheric Research, Boulder, Colorado*

(Manuscript received 29 May 2003, in final form 5 March 2004)

ABSTRACT

This paper discusses a large-scale modeling system with explicit representation of small-scale and mesoscale processes provided by a cloud-resolving model embedded in each column of a large-scale model, the superparameterization. In the original formulation, referred to as the cloud-resolving convection parameterization (CRCP), thermodynamic variables were coupled using appropriate averaging procedure, but horizontal momenta were coupled only through the relaxation approach. The improved system is based on the general formulation of the coupling between the two models, and the relaxation technique is abandoned. A simple but robust time integration scheme for the system is developed using the nonoscillatory forward-in-time approach applied in both the large-scale and cloud-scale models.

The improved formulation is applied to the problem, previously studied by the author, of large-scale organization of equatorial convection on a rotating constant sea surface temperature (SST) aquaplanet in convective–radiative quasi equilibrium. Three simulations are performed using 2D small-scale models as in the original CRCP approach. In the first two simulations, the 2D models have zonal orientation. The first simulation applies the new coupling scheme in the physical setup, which does not include surface drag. Tight coupling between large-scale and small-scale horizontal momenta results in rapid organization of Madden–Julian oscillation (MJO)-like coherent structures and development of strong superrotation. In the second simulation, surface drag is added into 2D small-scale model physics. This results in the development of MJO-like coherent structures with weak superrotation and more realistic strength of the westerly wind burst when compared to the terrestrial MJO. Surface drag is also included in the third simulation, where the coupling is formulated in such a way that orientation of 2D small-scale model domains is along the lower-tropospheric winds and thus it varies in space and time. Results from the third simulation are qualitatively similar to the simulation with surface drag and zonal orientation of small-scale models.

1. Introduction

Atmospheric processes of weather and climate cover about 10 decades of spatial scales, from a fraction of a millimeter (e.g., growth of cloud droplets and ice particles) to planetary (e.g., Hadley and Walker circulations). Regarding atmospheric fluid dynamics, one is primarily concerned with spatial scales larger than tens of meters because the smaller scales fall within the inertial range of atmospheric turbulence and can be modeled using subgrid-scale techniques used in large-eddy simulations (cf. Domaradzki and Adams 2002 and references therein). Spatial scales between 100 m and 100 km, referred to as small through mesoscale, show an abundance of processes associated with dry and moist convection, clouds, waves, boundary layer, topographic, and frontal circulations. Contemporary climate models have to rely on subgrid-scale parameterizations to represent these small-scale and mesoscale processes and interactions among them. These processes are often the key to climate dynamics and climate change—moist convection is likely the best example.

Cloud-system-resolving models (i.e., models with horizontal grid spacing of about 1 km) realistically represent small-scale and mesoscale processes. Intercomparisons with single-column models driven by large-scale forcing derived from field observations demonstrate that cloud-system-resolving models, even when applied in a simplified 2D slab-symmetric geometry, provide a superior representation of small-scale and mesoscale processes than do single-column models (e.g., Grabowski et al. 1996, 1998; Krueger and Lazarus 1999; Wu et al. 1998, 1999; Wu and Moncrieff 2001, Xie et al. 2002; Xu et al. 2002)[1]. A *global* cloud-system-resolving model, feasible on the largest modern computers, is 5 to 6 orders of magnitude more computationally

* The National Center for Atmospheric Research is sponsored by the National Science Foundation.

Corresponding author address: Dr. Wojciech W. Grabowski, NCAR, P.O. Box 3000, Boulder, CO 80307-3000.
E-mail: grabow@ncar.ucar.edu

[1] Much of the impetus for such intercomparisons comes from projects within the Global Energy and Water Cycle Experiment (GEWEX) Cloud System Study (GCSS; e.g., Moncrieff et al. 1997; Randall et al. 2003b).

demanding than traditional climate models and cannot be applied to climate simulations within the near future.

A different modeling approach, the cloud-resolving convection parameterization (CRCP) or ''superparameterization,'' was recently developed (Grabowski and Smolarkiewicz 1999; Grabowski 2001). The idea is to use a 2D cloud-system-resolving model in each column of a large-scale model to explicitly represent small-scale and mesoscale processes and interactions among them. This approach, two to three orders of magnitude more expensive than current climate models (Khairoutdinov and Randall 2001), is ideal for parallel computations and it can easily be implemented on supercomputers with thousands of processors (cf. Randall et al. 2003a).

The purpose of this paper is to present an improved large-scale modeling system with superparameterization. Emphasis is on the coupling of the large-scale and small-scale models, particularly for the momentum, which featured a relaxation between CRCP and global model momenta with a 1-h time scale.[2] The coupling discussed herein can be applied using either 2D or 3D geometry of the embedded small-scale model. In the 2D case, orientation of the embedded small-scale models becomes an issue. The orientation was zonal in Grabowski (2001, 2003a,b) and in Khairoutdinov and Randall (2001). A test with a meridional orientation was discussed in Grabowski (2002). The difference between results using zonal and meridional orientations of embedded 2D models was interpreted in Grabowski (2002) as the impact of convective transport of zonal momentum on the large-scale flow. Herein, a more general approach will be presented, where the orientation of the small-scale model inside a given large-scale model column changes as the large-scale winds evolve.

The relaxation approach using a time scale of a few hours proposed by Grabowski and Smolarkiewicz (1999) and Grabowski (2001) to couple horizontal momenta between large-scale and small-scale models seems sufficient to illustrate usefulness of the superparameterization for climate modeling (cf. Grabowski 2003a,b; Randall et al. 2003a). However, the relaxation technique is difficult to accept from the point of view of model energetics and, in the long run, one must consider a more rigorous approach to couple the large-scale and small-scale models. Such an approach is discussed in this paper.

One can also ask whether further development of the superparameterization using 2D framework, especially from the point of view of the large-scale momentum budget, can be justified. As discussed in Randall et al. (2003a), the main advantage of the superparameterization is to provide a realistic representation of the latent heating by small-scale processes and realistic spatial distribution of clouds (cloud overlap in particular), which is crucial for the radiative transfer. These can be viewed as ''thermodynamic factors'' through which small-scale processes impact the large-scale dynamics. Direct coupling between small-scale and large-scale momenta brings in the ''dynamic factor.''[3] The central issue is whether using embedded 2D small-scale models can be justified when not only thermodynamic fields but also horizontal momenta are directly coupled.

Previous studies suggest that 2D cloud-system-resolving models can provide a meaningful representation of the impact of deep convection on the momentum field, at least in selected situations (e.g., LeMone and Moncrieff 1994; Mapes and Wu 2001). It would be naive, however, to expect that such a statement is true in general. For instance, long 2D simulations tend to excite oscillatory patterns in the mean flow, presumably due to exaggerated wave–mean flow interactions in two spatial dimensions (cf. Held et al. 1993). As far as convective momentum transport is concerned, organized convection and mesoscale dynamics are key (e.g., Moncrieff 1981, 1992, 2004; Wu and Moncrieff 1996; Houze et al. 2000; Grabowski and Moncrieff 2001). The role of organized convection in the large-scale momentum budget has been argued for decades (e.g., Moncrieff 1981), but this issue is far from being resolved. Mesoscale circulations associated with organized convection feature a large aspect ratio (i.e., horizontal extent is much larger than the vertical) and simple (''archetypal'') 2D models have been argued to provide a useful basis for their transport properties (Moncrieff 1992; LeMone and Moncrieff 1994). However, even for systems with aspect ratios close to unity, such as convective boundary layer eddies, 2D dynamics provide a meaningful representation of their transports provided that the orientation of the 2D domain is carefully chosen (Moeng et al. 2004). In more basic terms, Werne (1993) has shown that, despite dramatic structural differences between two-and three-dimensional turbulent flows, the two-dimensional framework provides a useful basis for the hard-turbulent scaling of convective heat transfer.

One may also consider replacing the 2D superparameterization model with a 3D model. For instance, computational cost of the superparameterization using a 3D model with the same number of columns as the 2D model (e.g., 20 by 20 in 3D versus 400 in 2D) would be approximately the same. The key point is, however, that such a small 3D domain excludes mesoscale dynamics, which is an important motivation for the superparameterization as discussed above. If a 3D model with domain size appropriate for mesoscale dynamics

[2] In the implementation of this approach to the climate model illustrated in Khairoutdinov and Randall (2001) and in Randall et al. (2003a), only small-scale flow was relaxed toward the large-scale zonal flow. No relaxation of the large-scale flow toward the small-scale horizontal flow was allowed (i.e., no small-scale feedback; M. Khairoutdinov 2003, personal communication).

[3] From the point of view of the discussion later in the paper, it is worthwhile to point out that surface processes include fluxes of heat and momentum, and thus combine some of the thermodynamic and dynamic factors.

is used (say, 400 by 400 columns), the computational advantage over a fully cloud-system-resolving large-scale model will be small. Consequently, further development and testing of the superparameterization approach using a 2D small-scale model is justifiable, even if one is skeptical about the validity of the 2D approach from the point of view of the large-scale momentum budget.

The ultimate test for the superparameterization must come from a series of ''Big-Brother Experiments'' (Denis et al. 2002) where simulations applying superparameterization can be rigorously compared with 3D simulations applying horizontal resolution of, say, 1 km. Grabowski and Smolarkiewicz (1999, section 3) briefly discussed such a comparison for the case of tropical convection using the Global Atmospheric Research Program (GARP) Atlantic Tropical Experiment (GATE) data. Similar comparison in 2D was discussed in section 3 of Grabowski (2001). More tests of this kind are needed, especially for extratropical convection where rotational effects are important.

The next section discusses the generalized framework of the superparameterization and details a time integration scheme for the coupled system. The scheme is applied to the idealized problem of radiative–convective quasi equilibrium on a rotating constant sea surface temperature (SST) aquaplanet investigated previously (Grabowski 2001, 2002, 2003a,b). Model results are discussed in section 3. Conclusions and outlook are presented in section 4.

2. Mathematical formulation and the time-stepping algorithm

a. Coupling between large-scale and small-scale models

The superparameterization strategy, motivated by cloud-resolving simulations of tropical convection (e.g., Grabowski et al. 1996, 1998; Wu et al. 1998, 1999) is to apply a cloud-system-resolving model in each column of a large-scale model to explicitly represent small- and mesoscale processes that cannot be resolved by the large-scale model. The coupling formalism developed below applies to both 2D and 3D small-scale models applied as the superparameterization.

In the original CRCP, the 2D slab-symmetric small-scale model applies periodic lateral boundary conditions, which is convenient because of the energy and water conservation considerations. However, this implies that the domain-averaged vertical velocity of the subgrid-scale model must vanish and the vertical velocity field of the large-scale host model and small-scale subgrid-scale model must differ. In practice, this is not a significant limitation because vertical transport in the small-scale model is dominated by correlations between small-scale vertical velocity and small-scale perturbations of scalar variables. In other words, the impact of mean vertical velocity on small-scale fluctuations can be neglected based on the scale separation assumption, the cornerstone of any convection parameterization scheme, including CRCP (e.g., Arakawa and Schubert 1974; section 2 in Grabowski et al. 1996).

It is possible to design an approach in which lateral boundary conditions for the small-scale model are formulated differently and vertical velocities between the two models are coupled (see a discussion in Randall et al. 2003a). However, such an approach requires special treatment of inflow and outflow boundary conditions among small-scale models from neighboring columns of the host model in order to conserve water and energy. Such an approach is cumbersome if the superparameterization uses 3D model or if orientation of 2D models is allowed to vary in time and space. Consequently, it is assumed throughout this paper that the superparameterization applies the cloud-system-resolving model with periodic (doubly periodic in 3D) lateral boundary conditions and that the coupling described herein applies only to the thermodynamic variables and horizontal momenta. One needs to keep in mind, however, that such a formulation strongly limits the propagation of small-scale features across the large-scale model grid (cf. section 3 in Grabowski 2001).

Superparameterization involves application of two models and two sets of model variables. The variables applied to represent large-scale processes are $Q \equiv Q(X, Y, Z, t)$ (e.g., horizontal velocity component, temperature, water vapor mixing ratio, etc) in the 3D coordinates of the large-scale model (X, Y, Z): Q includes collective effects of small-scale processes that are considered in the small-scale model. The corresponding small-scale model variables $q \equiv q(x, y, z, t)|_{(X,Y)}$ represent small-scale variability of the large-scale variable Q in a 3D small-scale domain embedded within the large-scale model column at (X, Y). If a 2D cloud system-resolving model is used, as in the original CRCP approach, the small-scale variables $q \equiv q(x, z, t)|_{(X,Y)}$ represent small-scale variability of the large-scale variable Q in the vertical plane (x, z) embedded within the large-scale model column at (X, Y). The small-scale variable represents subgrid-scale variability of Q and it also has to include effects of large-scale processes.

The fundamental property of the two sets of variables is that the horizontal average of the small-scale variable q within a single column of a large-scale model is exactly equal to the large-scale variable Q at this level. This highlights the coupling between the two models and is schematically expressed as

$$Q(X, Y, Z, t) = \langle q(x, y, z, t)|_{(X,Y)} \rangle, \qquad (1)$$

where the small-scale model levels correspond to the levels of the large-scale model ($z \equiv Z$).The operator $\langle\ \rangle$ denotes the horizontal averaging of a small-scale dependent variable, for example,

$$\langle q(x, y, z, t)|_{(X,Y)}\rangle \equiv \frac{1}{L_x L_y}\int_{-L_x/2}^{L_x/2}\int_{-L_y/2}^{L_y/2} q(\xi, \zeta, z, t)|_{(X,Y)}\, d\zeta\, d\xi, \quad (2)$$

where L_x and L_y describe the extent of the 3D horizontal domain used in each small-scale model. For the 2D small-scale model, (2) involves only a single integral. Equation (1) is abbreviated as $Q = \langle q\rangle$.

The coupling of the large-scale host model and small-scale subgrid-scale model is now explained. The large-scale model equations can be schematically represented as

$$\frac{\partial Q}{\partial t} = A_Q + S_Q + F^Q_{\rm SS}, \quad (3a)$$

where $A_Q \equiv -\mathbf{U}\cdot\boldsymbol{\nabla}Q$ is the large-scale advection term ($\mathbf{U}$ is the large-scale flow), S_Q is its large-scale source (e.g., pressure gradient or Coriolis acceleration for horizontal flow velocity, large-scale dissipative terms for scalars, etc.), and $F^Q_{\rm SS}(X, Y, Z, t)$ is the source due to small-scale processes that are considered in the small-scale model. This term was referred to as the small-scale model feedback in Grabowski and Smolarkiewicz (1999) and Grabowski (2001).

Similarly, the small-scale model equations are

$$\frac{\partial q}{\partial t} = a_q + s_q + f^q_{\rm LS}, \quad (3b)$$

where $a_q \equiv -\mathbf{u}\cdot\boldsymbol{\nabla}q$ ($\mathbf{u}$ is the small-scale flow), s_q represents small-scale sources (e.g., surface drag for velocity or latent heating due to phase changes for the temperature), and $f^q_{\rm LS}(z, t)$ is the large-scale forcing for the small-scale model. This term is applied homogeneously across the entire computational domain at a given level (cf. Grabowski et al. 1996). In general, the large-scale and small-scale model equations can be different. For instance, the large-scale model can apply hydrostatic primitive equations (cf. Khairoutdinov and Randall 2001), whereas the small-scale model requires equations appropriate for small-scale nonhydrostatic dynamics.

The change of the large-scale variable comes from the combined effect of the large-scale transport and sources $A_Q + S_Q$ and the averaged subgrid-scale transport and sources $\langle a_q\rangle + \langle s_q\rangle$. Because of (1), this change can be represented by using either the large-scale variable Q or the averaged small-scale variable $\langle q\rangle$. It follows that

$$\frac{\partial Q}{\partial t} = \frac{\partial\langle q\rangle}{\partial t} = A_Q + S_Q + \langle a_q\rangle + \langle s_q\rangle. \quad (4)$$

Comparing (3) and (4) allows one to deduce the form of the coupling terms $F^Q_{\rm SS}$ and $f^q_{\rm LS}$. The key is that $F^Q_{\rm SS}$ involves only small-scale variables and $f^q_{\rm LS}$ only large-scale variables. The only possibility for (4) to match (3) in such a case is that

$$F^Q_{\rm SS} = \langle a_q\rangle + \langle s_q\rangle \quad (5a)$$

$$f^q_{\rm LS} = A_Q + S_Q. \quad (5b)$$

b. Numerical algorithm

Depending upon the particular algorithms applied to integrate large-scale and small-scale models, various approaches to implement (3) and (5) can be designed. Herein, we detail an algorithm for the nonoscillatory forward-in-time scheme developed by Smolarkiewicz and Margolin (1998 and references therein) and applied in both the small-scale model (Smolarkiewicz and Margolin 1997) and the large-scale model (Smolarkiewicz et al. 2001; Grabowski and Smolarkiewicz 2002). The key is that the algorithm strictly enforces (1) for the small-scale variables only. The large-scale model is advanced first using the most recent small-scale model feedback and updated large-scale forcing is used to advance the small-scale model.

In the following, we first describe the numerical algorithm and later show that it results in the time integration scheme where $\langle q\rangle$ follows (4). The algorithm proceeds from time level n to $n + 1$ over the large-scale model time step ΔT as follows.

1) LARGE-SCALE MODEL TIME STEP

With the small-scale model feedback at time level n denoted as $F^Q_{\rm SS}|^{(n)}$, the forward-in-time integration of large-scale model (3a) proceeds as

$$Q|^{(n+1)} = Q|^{(n)} + \Delta T(A_Q + S_Q)|^{n+1}_n + \Delta T F^Q_{\rm SS}|^{(n)}, \quad (6)$$

where the second term on rhs of (6) is a schematic representation of the numerical algorithm applied in the large-scale model. Note that (6) is uncentered in time because the small-scale feedback at $n + 1$ is not included in (6).

2) SMALL-SCALE MODEL TIME STEP

After completing the large-scale model time step (6), the small-scale model is integrated over several smaller time steps to advance from an n to $n + 1$ time level. At the beginning of small-scale model calculations, the large-scale forcing is calculated according to

$$f^q_{\rm LS} = \frac{Q|^{(n+1)} - \langle q|^{(n)}\rangle}{\Delta T}. \quad (7)$$

Subsequently, the small-scale model (3b) is integrated forward in time using a smaller time step Δt. At each small-scale model time step, the large-scale forcing (7) is kept constant and, at each height, it is applied homogeneously across the entire computational domain of the small-scale model as in cloud-resolving simulations driven by observed large-scale conditions (cf. Grabowski et al. 1996). The final small-scale solution of (3b) at the $n + 1$ time level can be written as

$$q|^{(n+1)} = q|^{(n)} + \sum_{i=1}^{N} \Delta t(a_q + s_q)|_i^{i+1} + \sum_{i=1}^{N} \Delta t f_{\mathrm{LS}}^{q}, \quad (8)$$

where $N = \Delta T/\Delta t$ and, similar to (6), the second term is a schematic representation of the numerical algorithm applied in the small-scale model. Finally, the small-scale feedback is updated as

$$F_{\mathrm{SS}}^{Q}|^{(n+1)} = \frac{\langle q|^{(n+1)}\rangle - Q|^{(n+1)}}{\Delta T}. \quad (9)$$

The finite difference form of coupling terms (7) and (9) is a relaxation with the time scale equal to the large-scale model time step ΔT. This may seem inconsistent with the criticism of the relaxation technique presented in the introduction. However, the key is that application of these terms to the coupled system results in the time integration scheme, which is consistent with (4). To demonstrate this, one needs to use (9) for $F_{\mathrm{SS}}^{Q}|^{(n)}$ and apply it to (6) to obtain the large-scale variable at the $n + 1$ time level. The result is

$$Q|^{(n+1)} = \langle q|^{(n)}\rangle + \Delta T(A_Q + S_Q)|_n^{n+1}. \quad (10)$$

Similarly, using (10) in (7) and (8), one obtains the mean small-scale variable at the $n + 1$ time level as

$$\langle q|^{(n+1)}\rangle = \langle q|^{(n)}\rangle + \sum_{i=1}^{N} \Delta t\langle(a_q + s_q)|_i^{i+1}\rangle + \Delta T(A_Q + S_Q)|_n^{n+1}. \quad (11)$$

It follows that only the *mean small-scale variables* are *consistent with* (4). The large-scale variables, on the other hand, do not include the small-scale feedback at the $n + 1$ time level yet [i.e., the middle term on rhs of (11)]. However, the updated small-scale feedback term (9) tends to correct the discrepancy between $Q|^{(n+1)}$ and $\langle q|^{(n+1)}\rangle$ in the subsequent time step. Another way to look at the scheme (6)–(9) is to compare it to the predictor–corrector technique, where large-scale equations correspond to the predictor step because they are solved using an uncentered-in-time scheme (6), whereas small-scale equations form a corrector step. Equations (10) and (11) stress the significance of the small-scale variables that include all the required sources at the $n + 1$ time level.

Application of the algorithm (6)–(9) for scalar variables is straightforward. As far as horizontal momenta are concerned, the algorithm is also straightforward when a 3D cloud-system-resolving model is used. However, for the 2D model, horizontal momenta require special attention, especially when the model's orientation within the large-scale model column changes as the integration progresses. In the latter case, the coupling of the horizontal momenta is accomplished in the following manner: First, the large-scale model is advanced according to (6). Next, a new orientation of the small-scale model is calculated based on the updated large-scale wind. Subsequently, the large-scale horizontal wind at all model levels is decomposed into components parallel and perpendicular to the new orientation of the small-scale model. The two components are used in the small-scale model to derive the new large-scale forcing (7) for the wind component along the computational domain (i.e., that includes the small-scale fluctuations) and the perpendicular one (i.e., that has no dynamical role in small-scale calculations and is treated as a passive scalar). The small-scale calculations then proceed until the $n + 1$ time level is reached [cf. (8)]. At this time, the new small-scale feedback terms (9) are calculated, separately for the wind component parallel and perpendicular to the orientation of the computational domain. Finally, the feedback terms are transformed back into the coordinate system of the large-scale model (i.e., zonal and meridional) to be applied in a subsequent time step.

In the case when the 2D small-scale model changes its orientation between subsequent time steps, the algorithm outlined above implies that the small-scale thermodynamic fields (clouds in particular) are the same before and after the change of the model orientation. In other words, the only impact of the new orientation of the 2D computational domain on the small-scale fields within the small-scale model occurs through the wind tendencies (7) that the small-scale model experiences. For instance, in a hypothetical situation when the large-scale wind does not change but the orientation of the domain changes, the only impact the small-scale fields experience is the change of the mean wind along the computational domain.

3. MJO-like systems on a rotating constant SST aquaplanet

Following Grabowski (2001, 2002, 2003a, hereafter referred to as G01, G02, and G03, respectively), we consider an idealized problem of large-scale organization of equatorial convection on a constant-SST (30°C) aquaplanet, with the same size and rotation as the earth. The simulations closely follow G01 (section 4; subsequently referred to as EW in G02 and CTRL in G03) except for the new coupling between the models as described above, inclusion of the surface drag into the model physics, and variable orientation of the computational domain of 2D cloud-system-resolving models. Only a brief description of the problem, numerical models, and the modeling setup is presented here.

The global model is the anelastic nonhydrostatic two-time-level nonoscillatory forward-in-time Eulerian model in spherical geometry (Smolarkiewicz et al. 2001; Grabowski and Smolarkiewicz 2002) applying a low horizontal resolution (32 × 16), with 51 levels in the vertical and a uniform vertical gridlength of 0.5 km. The global model time step is 12 min. The two-dimensional anelastic small-scale model embedded in each column of the global model has horizontal periodic domain of 200 km with a 2-km grid length and the same

TABLE 1. Numerical simulations discussed in this paper.

	Orientation of cloud-scale domains	Surface drag
EW-NSD	E–W	No
EW-SD	E–W	Yes
VAR-SD	Along lower-tropospheric wind	Yes

vertical grid as in the global model. The cloud model time step is 20 s. Prescribed radiative cooling is applied as in G01 and G02 (i.e., -1.5 K day^{-1} below 12 km, linearly decreasing to zero between 12 and 15 km, and zero above 15 km). The simulations are initiated with no large-scale flow, and a snapshot from a single small-scale model integration of a convective–radiative quasi equilibrium initiates the 2D small-scale models (see section 4 of G01 for details). As in G01, G02, and G03, the simulations are run for 80 days.

Three simulations are discussed (see Table 1). In all of them, the coupling and time integration presented in G01 is replaced by the scheme outlined in the previous section. The first simulation, referred to as EW-NSD (E–W orientation, no surface drag), has the same setup as in G01, that is, the orientation of 2D small-scale domains is east–west. Because of the new time integration scheme, it features tight coupling between horizontal momenta of the two models because 1-h relaxation used in G01, G02, and G03 is replaced by the coupling (7) and (9). The only difference between EW-NSD and the second simulation, EW-SD (E–W orientation, with surface drag), is that the surface drag is added into the model physics. The surface drag is included in the small-scale model in the same fashion as surface latent and sensible heat fluxes, that is, by calculating the surface fluxes using bulk approach (see appendix C in Grabowski et al. 1996) and distributing these fluxes in the lowest 600 m of the troposphere. The third simulation, VAR-SD (variable orientation, with surface drag), is similar to EW-SD, but the orientation of the superparameterization domains is allowed to vary. The orientation is selected along the mean wind in the lowest 4 km. The motivation is to include topographic effects into the physics of 2D small-scale models in the future. Arguably, one can also consider aligning the 2D domains along the low-level shear.

Figure 1, to be compared with G03 Fig. 1 for the simulation CTRL, shows the Hovmöller (time–space) diagrams of the surface precipitation and precipitable water at the equator for the duration of the simulation EW-NSD. Zonal distributions of surface precipitation and precipitable water at a given latitude and at a given time are obtained by combining cloud-scale data from small-scale model domains located at this latitude. Because CRCP domains have smaller horizontal extent than the zonal grid spacing of the large-scale model near the equator, the finescale precipitation pattern is not to scale (this comment also applies to similar plots shown in G01, G02, and G03). The precipitable water plot uses averages from CRCP domains. The figure also shows snapshots of vertical and horizontal flow in the vertical equatorial plane, as well as the distribution of the surface precipitation and the total surface flux along the equator, at day 80.

The figure illustrates that the new coupling between large-scale and small-scale models results in faster development of the MJO-like coherent structure than in CTRL of G03 around day 20 versus around day 50) and that the structure seems to propagate faster in the second half of the simulation EW-NSD. The apparent increase of the propagation speed comes from the development of the mean westerly flow within the equatorial waveguide, the superrotation (cf. section 5d in G03). This is illustrated in Fig. 2, which shows that the superrotation is stronger with the new coupling when compared to simulations discussed in G02 and G03. This is expected because, as argued by Moncrieff (2004), the superrotation results from the impact of MJO-like coherent structures on the mean zonal momentum. Tight coupling between large-scale and small-scale models likely enhances the development of superrotation.

Figure 3 shows snapshots of the longitude–latitude distribution of surface precipitation and surface zonal winds for EW-NSD at day 40 and day 80. At day 40, the MJO-like coherent structure is present in the western part of the waveguide and it features leading-edge convection in the center of the domain and westerly flow at the surface (the westerly wind burst) westward of the maximum surface precipitation. The figure supports a conjecture that the large-scale perturbations of precipitation and precipitable water illustrated in Fig. 1 are indeed associated with the MJO-like coherent structures, at least around day 40. The structures at day 80 are considerably distorted. Arguably, this distortion, together with numerical diffusion, results in the stabilization of the superrotation in the last 20 days of the simulation as shown in Fig. 2.

Because EW-NSD does not include any dissipative processes that may control the strength of the flow (except for the numerical diffusion), results of this simulation may be considered unrealistic. In reality, surface drag has significant control over the large-scale flow. For instance, strong impact of the surface drag on baroclinic waves was demonstrated in Rotunno et al. (1998). This is the motivation behind the simulation EW-SD. Results are illustrated in Figs. 4 and 5. These figures, in the same format as Figs. 1 and 3 for EW-NSD, illustrate the large-scale organization of equatorial convection in EW-SD. Including surface drag results in MJO-like coherent structures similar to the results presented in G01, G02, and G03. However, the strength of the superrotation (cf. Fig. 6), as well as the strength of the surface westerly winds behind the leading-edge deep convection are significantly reduced (surface westerly winds in EW-SD seldom exceed 10 m s^{-1}). This is consistent with observations of the terrestrial MJO (Lin and Johnson 1996, their Fig. 16).

Figure 7, in the same format as Figs. 1 and 4, illus-

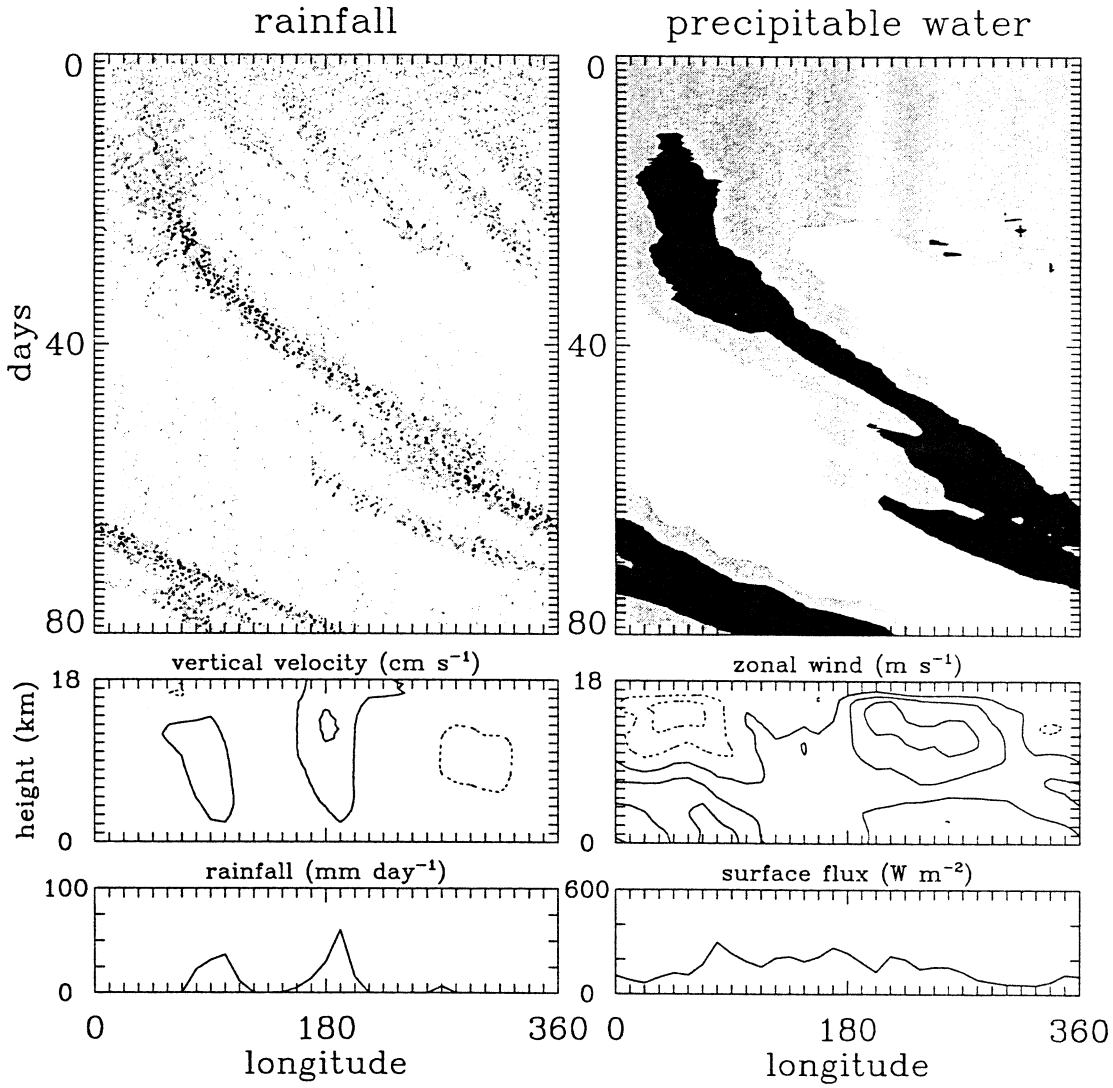

FIG. 1. Results from EW-NSD. (top) Hovmöller diagrams of the (upper left) surface precipitation and (upper right) precipitable water at the equator. Precipitation intensities larger than 0.2 and 5 mm h^{-1} are shown using gray and black shading, respectively. Precipitable water smaller (larger) than 65 (75) kg m^{-2} is shown as white (black); gray shading is for precipitable water between 65 and 75 kg m^{-2}. (middle) (left) Vertical and (right) horizontal velocities in the vertical plane at the equator at day 80. Contour interval is 2 cm s^{-1} (10 m s^{-1}) for vertical (horizontal) velocities starting at 1 cm s^{-1} (5 m s^{-1}); solid (dashed) contours are for positive (negative) values. (bottom) Spatial distribution of (lower left) the surface precipitation and (lower right) the sum of surface sensible and latent heat fluxes along the equator, also at day 80.

trates results for the simulation VAR-SD. In general, allowing 2D domains to be aligned along the lower-tropospheric winds results in MJO-like coherence similar to the simulation with domains aligned east–west (EW-SD). In particular, the propagation speed is approximately the same as is the superrotation (cf. Fig. 6). There are, however, some differences. First, VAR-SD results is a single MJO-like coherent structure, whereas EW-SD seems to have two of them. This may be just a coincidence and the two simulations may simply represent two possible realizations of the MJO-like coherence (see results discussed in G02 and G03). Moreover, there are differences in the surface precipitation ahead and behind of the MJO-like coherent structure. In VAR-SD (in contrast to simulations described in G03, e.g., CTRL), the region behind the MJO lacks deep convection. This impacts the zonal gradient of precipitable water ahead of and behind the maximum surface precipitation. The asymmetry of the zonal gradient of the precipitable water is perhaps most evident in VAR-SD (see Fig. 7), but it is also present during some periods in EW-SD (e.g., around day 40 in Fig. 4). Such a difference in surface precipitation and precipitable water is likely a result of low-level shear present behind the leading edge convection when the surface drag is included in the model equations, as shown in zonal wind

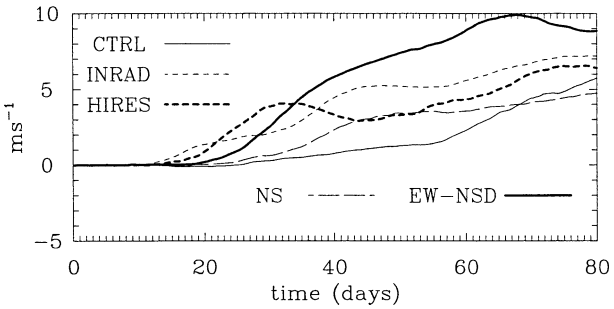

FIG. 2. Evolution of the density-weighted zonal flow on the equator for the simulation EW-NSD and for G03 simulations CTRL, INRAD (similar to CTRL, but with interactive radiation replacing prescribed radiative cooling), and HIRES (similar to CTRL, but using higher horizontal resolution of the global model), and from G02 simulation NS (similar to CTRL, but with small-scale models aligned north–south).

plots in Figs. 4 and 7. Although the prominence of shallow convection in the westerly wind burst area is supported by observations (Lin and Johnson 1996, their Fig. 16), the vertical resolution of the model is too low to confidently treat this aspect of model results.

Spatial distribution of the surface precipitation and the surface zonal wind in VAR-SD at day 80 is illustrated in Fig. 8. The MJO-like coherent structure is located in the eastern part of the domain. The strength of the westerly wind burst is similar to the simulation EW-SD and much weaker than at day 40 of EW-NSD. The figure also shows orientations of computational domains of the 2D small-scale models at this time. Within the equatorial waveguide, the orientation is mostly zonal because of the prevailing large-scale winds. This is also the direction of the prevailing low-level shear. Outside the equatorial waveguide, on the other hand, the orientation varies significantly in space (and in time, not shown) because of light winds outside of the waveguide.

4. Discussion and conclusions

This paper discusses an improved strategy for representing small-scale and mesoscale processes in large-scale models of weather and climate by embedding a cloud-system-resolving model in each column of the large-scale model. This approach, referred to as the superparameterization, follows the cloud-resolving convection parameterization (CRCP; Grabowski and Smolarkiewicz 1999; Grabowski 2001, 2002, 2003a,b), which was proposed to improve representation of deep convection. CRCP was motivated by cloud-resolving simulations of tropical convection driven by observed large-scale conditions. Superparameterization provides

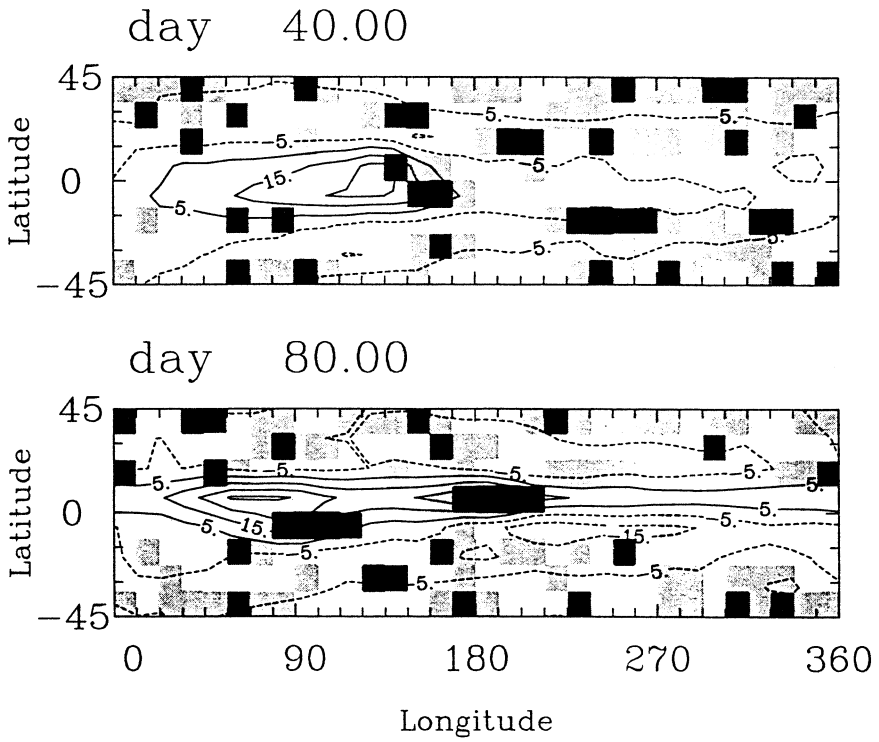

FIG. 3. Instantaneous fields for EW-NSD (top) at day 40 and (bottom) at day 80 of the surface zonal winds (solid and dashed contours for positive and negative values, respectively; contour interval of 10 m s^{-1} starting at 5 m s^{-1}) and spatial distributions of the surface precipitation rate derived from small-scale model data (gray shading; precipitation rate larger than 1.5 and 15 mm h^{-1} is shown using light and dark shading, respectively). The plots show data from the zonal belt between 45°S and 45°N only.

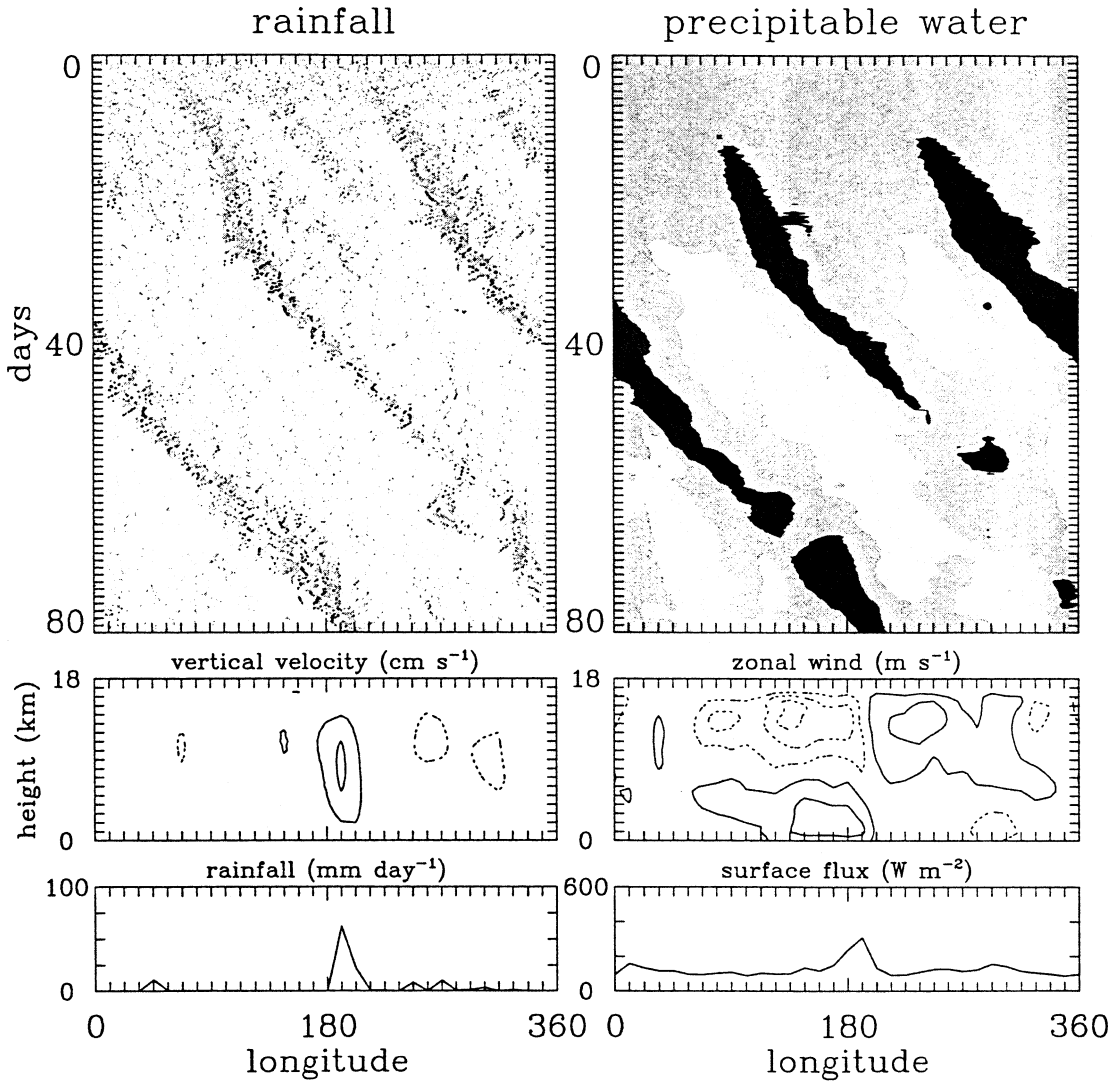

FIG. 4. As in Fig. 1 but for EW-SD.

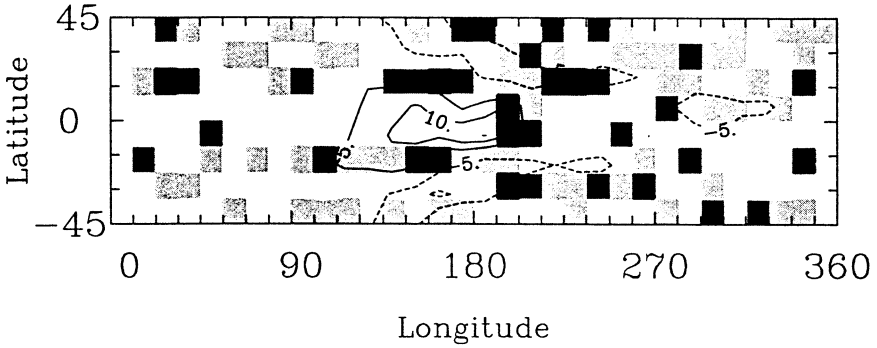

FIG. 5. As in Fig. 3 but for day 80 of EW-SD. Contour interval is 5 m s^{-1}, and zero contour is not shown.

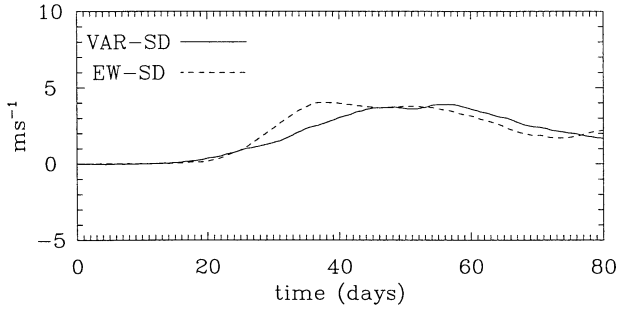

FIG. 6. As in Fig. 2 but for EW-SD and VAR-SD.

encouraging results when applied to the global model of the terrestrial climate (Khairoutdinov and Randall 2001; Randall et al. 2003a). Improved representation of other small-scale and mesoscale processes, besides deep convection, is possible using this approach when such processes are included in the framework of the small-scale model. Radiative transfer (cf. Grabowski 2003b), boundary layer processes, land surface processes, and topography are pertinent examples.

In the original formulation of CRCP (Grabowski and Smolarkiewicz 1999; Grabowski 2001), the coupling between large-scale and small-scale models was different for thermodynamic fields and horizontal momenta. Averaged small-scale thermodynamic fields were used in the large-scale model and relaxation (with a 1-h time scale) was applied to couple the horizontal momenta between the two models. Relaxation approach, perhaps appropriate to illustrate the potential of the superparameterization, is questionable in climate simulations. For instance, it is difficult (perhaps impossible) to analyze model energetics when relaxation is used because such an approach results in the unphysical transfer of kinetic energy between large-scale and small-scale flows. Con-

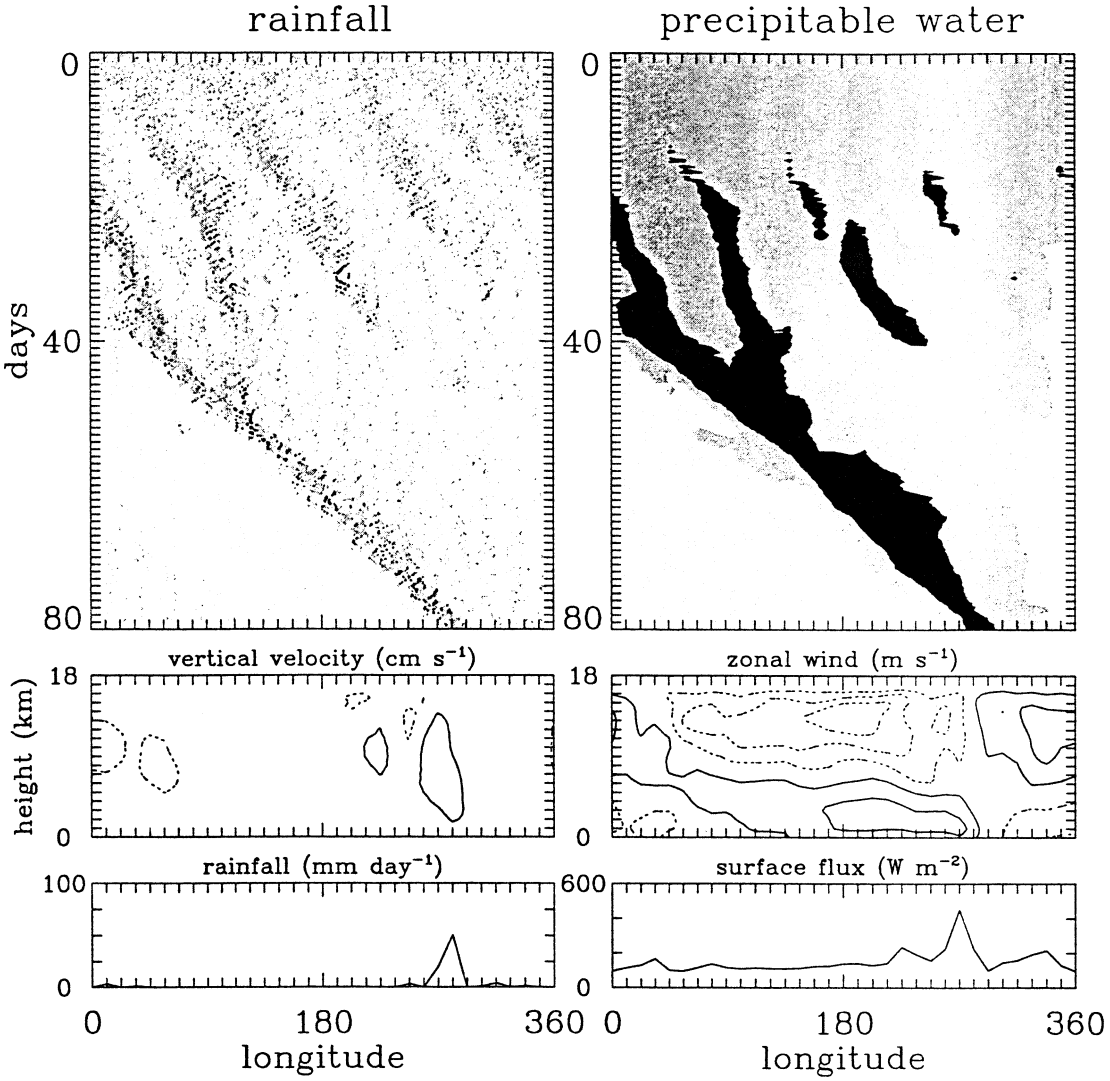

FIG. 7. As in Fig. 1 but for VAR-SD.

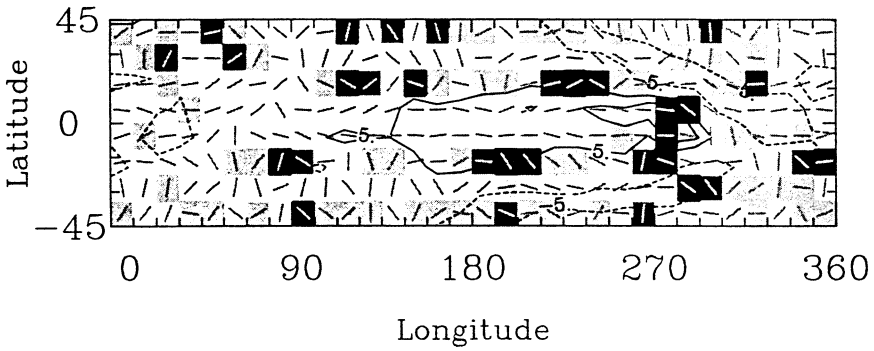

FIG. 8. As in Fig. 5 but for day 80 of VAR-SD. Orientation of small-scale model domains is along the bar shown in each large-scale model column.

sequently, the coupling proposed previously needs to be improved and horizontal momenta, not only thermodynamic fields, need to be directly coupled between small-scale and large-scale models. The direct coupling means that, at every model time step, the horizontally averaged small-scale variable is exactly equal to the large-scale variable for a given large-scale model column [cf. (1)]. With this assumption, a general coupling formalism can be developed (cf. section 2a). This formalism is applicable regardless of whether a 2D or 3D small-scale model is used.

Practical implementation of the general coupling depends on the time integration scheme applied by the two models. Herein, we develop a scheme for the case when both large-scale and small-scale models apply the nonoscillatory forward-in-time scheme developed by Smolarkiewicz and Margolin (1998 and references therein). The time integration scheme for the coupled system is straightforward: a large-scale model is advanced first using the most recent small-scale model feedback, and small-scale calculations follow with updated large-scale forcing. The scheme is in the spirit of the predictor–corrector technique, where the large-scale model integration corresponds to the predictor step, and the small-scale model integration represents the corrector step. As shown in section 2b, only small-scale variables at any given time level include all large-scale and small-scale sources and sinks. This highlights the importance of the small-scale model fields when the new time integration scheme is used.

The improved formulation is applied to the problem of large-scale organization of equatorial convection on a rotating constant-SST aquaplanet studied in Grabowski (2001, 2002, 2003a,b) using CRCP with 2D small-scale models. First, the new scheme is used in the physical setup, which does not include surface drag (i.e., the same as considered previously). Tight coupling between large-scale and small-scale horizontal momenta results in fast organization of the MJO-like coherent structure and development of strong superrotation within the equatorial waveguide in the second half of the simulation. The strong superrotation adversely impacts the coherence of MJO-like structures toward the end of this simulation. To control the superrotation, surface drag is added into the model physics and it is applied inside the 2D small-scale models. The result is the development of MJO-like coherent structures with more realistic strength of the westerly wind burst, to the west of the maximum surface precipitation, when compared to the terrestrial MJO (Lin and Johnson 1996, Fig. 16), and with weak superrotation. In the above two tests, zonal (i.e., E–W) orientation of small-scale model domains is used. In the final test, the coupling is formulated in such a way that small-scale domains are allowed to be aligned in any direction, the orientation can be different in different columns, and may change as the simulation progresses. Herein, the orientation is chosen along the lower-tropospheric winds. Results from a simulation with the surface drag and variable orientation are similar to the simulation when orientation is fixed, especially for the superrotation (cf. Fig. 6).

One can argue that, from the point of view of the dynamics of mesoscale convective systems, choosing the orientation of the small-scale model domains along the low-level shear, not along the low-level winds, would be more appropriate. In simulations discussed in this paper, such a change would probably have a minor impact because, within the equatorial waveguide, both lower-tropospheric wind and lower-tropospheric shear are predominantly zonal. Thus, current simulations are not particularly discriminating as far as the orientation is the 2D superparameterization model is concerned. This issue will be revisited in aquaplanet simulations using prescribed meridional distribution of zonally uniform SST (e.g., Hayashi and Sumi 1986). Since such a setup features Hadley circulation and extratropical baroclinic eddies, meridional distribution of the mean zonal flow as well as the strength of the mean meridional circulation may be sensitive to the orientation of superparameterization domains. Results of such simulations will be reported in the future.

The motivation for downwind orientation of small-scale domains comes from our intention to include topographic generation of small-scale gravity waves and

gravity wave drag in the future. Obviously, topographic waves are generated by the low-level flow over cross-wind topographic features. Downwind orientation of small-scale domains may also be important for the coupled atmosphere–ocean system. Since surface drag is a quadratic function of the surface wind speed (at least when drag coefficient is constant), resolving surface wind fluctuations in the direction along the mean surface wind is important for the credible estimate of the mean large-scale surface drag. The impact of small- and mesoscale fluctuations of surface winds on the surface heat fluxes is well recognized (e.g., Jabouille et al. 1996; Esbensen and McPhaden 1996; section 3d in Grabowski et al. 1998), but their effect on surface drag has received much less attention.

As discussed in the introduction, replacing 2D small-scale models with 3D models featuring a similar number of columns does not seem appealing because of the exclusion of mesoscale dynamics in such a case. However, one can envision using a quasi-3D model, where the horizontal extent of 3D domain is much larger in one direction than in the other (say, 200 by 20 columns). Such an approach has been used in cloud modeling (e.g., Tompkins 2001) and it allows capturing elements of mesoscale dynamics as well as three-dimensional effects of convective drafts. When used as the superparameterization, the quasi-3D domains would change orientation during model integration in such a way that the long edge of the quasi-3D domain would be aligned along the low-level shear. The coupling scheme developed in this paper allows integrating a system of equation describing the evolution of such a system. Clearly, many tests using different orientations of 2D domains and variety of 3D configurations need to be performed to fully explore capabilities offered by the superparameterization.

Proof-of-concept for the superparameterization requires further testing, most likely using the Big-Brother Experiments (Denis et al. 2002) as mentioned in the introduction. Moreover, additional small-scale and mesoscale processes need to be gradually included into the small-scale model framework. Processes currently under investigation include boundary layer dynamics and shallow convection. These are important for application of the superparameterization over land where surface forcing is strong and there is a pronounced diurnal cycle. Subsequently, land surface processes and topographically forced gravity waves will be explored. These investigations will be reported in forthcoming publications.

Acknowledgments. Comments on the manuscript by Mitch Moncrieff, Piotr Smolarkiewicz, and Steve Woolnough are acknowledged, as is the editing of the manuscript by Kay Sandoval. This work is supported by NCAR's Clouds in Climate Program (CCP). The National Center for Atmospheric Research is operated by the University Corporation for Atmospheric Research under sponsorship of the National Science Foundation.

REFERENCES

Arakawa, A., and W. H. Schubert, 1974: Interaction of a cumulus cloud ensemble with the large-scale environment. *J. Atmos. Sci.*, **31,** 674–701.

Denis, B., R. Laprise, D. Caya, and J. Cote, 2002: Downscaling ability of one-way nested regional climate models: The Big-Brother Experiment. *Climate Dyn.,* **18,** 627–646.

Domaradzki, J. A., and N. A. Adams, 2002: Direct modelling of subgrid scales of turbulence in large eddy simulations. *J. Turbulence,* **3,** 024, doi.10.1088/1468-5248/3/1/024.

Esbensen, S. K., and M. J. McPhaden, 1996: Enhancement of tropical ocean evaporation and sensible heat flux by atmospheric mesoscale systems. *J. Climate,* **9,** 2307–2325.

Grabowski, W. W., 2001: Coupling cloud processes with the large-scale dynamics using the cloud-resolving convection parameterization (CRCP). *J. Atmos. Sci.*, **58,** 978–997.

——, 2002: Large-scale organization of moist convection in idealized aquaplanet simulations. *Int. J. Numer. Methods Fluids,* **39,** 843–853.

——, 2003a: MJO-like coherent structures: Sensitivity simulations using the cloud-resolving convection parameterization (CRCP). *J. Atmos. Sci.,* **60,** 847–864.

——, 2003b: Impact of cloud microphysics on convective–radiative quasi equilibrium revealed by cloud-resolving convection parameterization (CRCP). *J. Climate,* **16,** 3463–3475.

——, and P. K. Smolarkiewicz, 1999: CRCP: A cloud resolving convection parameterization for modeling the tropical convecting atmosphere. *Physica D,* **133,** 171–178.

——, and M. W. Moncrieff, 2001: Large-scale organization of tropical convection in two-dimensional explicit numerical simulations. *Quart. J. Roy. Meteor. Soc.,* **127,** 445–468.

——, and P. K. Smolarkiewicz, 2002: A multiscale anelastic model for meteorological research. *Mon. Wea. Rev.,* **130,** 939–956.

——, X. Wu, and M. W. Moncrieff, 1996: Cloud-resolving modeling of tropical cloud systems during Phase III of GATE. Part I: Two-dimensional experiments. *J. Atmos. Sci.,* **53,** 3684–3709.

——, ——, ——, and W. D. Hall, 1998: Cloud-resolving modeling of tropical cloud systems during Phase III of GATE. Part II: Effects of resolution and the third spatial dimension. *J. Atmos. Sci.,* **55,** 3264–3282.

Hayashi, Y.-Y., and A. Sumi, 1986: The 30–40 day oscillations simulated in an ''aqua planet'' model. *J. Meteor. Soc. Japan,* **64,** 451–467.

Held, I. M., R. S. Hemler, and V. Ramaswamy, 1993: Radiative–convective equilibrium with explicit two-dimensional moist convection. *J. Atmos. Sci.,* **50,** 3909–3927.

Houze, R. A., Jr., S. S. Chen, D. E. Kingsmill, Y. Serra, and S. E. Yuter, 2000: Convection over the Pacific warm pool in relation to the atmospheric Kelvin–Rossby wave. *J. Atmos. Sci.,* **57,** 3058–3089.

Jabouille, P., J. L. Redelsperger, and J. P. Lafore, 1996: Modifications of surface fluxes by atmospheric convection in the TOGA COARE region. *Mon. Wea. Rev.,* **124,** 816–837.

Khairoutdinov, M. F., and D. A. Randall, 2001: A cloud resolving model as a cloud parameterization in the NCAR Community Climate System Model: Preliminary results. *Geophys. Res. Lett.,* **28,** 3617–3620.

Krueger, S. K., and S. M. Lazarus, 1999: Intercomparison of multi-day simulations of convection during TOGA COARE with several cloud-resolving and single-column models. Preprints, *23d Conf. on Hurricanes and Tropical Meteorology,* Dallas, TX, Amer. Meteor. Soc., 643–647.

LeMone, M. A., and M. W. Moncrieff, 1994: Momentum and mass transport by convective bands: Comparisons of highly idealized dynamical models to observations. *J. Atmos. Sci.,* **51,** 281–305.

Lin, X., and R. H. Johnson, 1996: Kinematic and thermodynamic characteristics of the flow over the western Pacific warm pool during TOGA COARE. *J. Atmos. Sci.,* **53,** 695–715.

Mapes, B. E., and X. Wu, 2001: Convective eddy momentum tendencies in long cloud-resolving model simulations. *J. Atmos. Sci.,* **58,** 517–526.

Moeng, C.-H., J. C. McWilliams, R. Rotunno, P. P. Sullivan, and J. Weil, 2004: Investigating 2D modeling of atmospheric convection in the PBL. *J. Atmos. Sci.,* **61,** 889–903.

Moncrieff, M. W., 1981: A theory of organized steady convection and its transport properties. *Quart. J. Roy. Meteor. Soc.,* **107,** 29–50.

——, 1992: Organized convective systems: Archetypal dynamical models, mass and momentum flux theory, and parameterization. *Quart. J. Roy. Meteor. Soc.,* **118,** 819–850.

——, 2004: Analytic representation of the large-scale organization of tropical convection. *J. Atmos. Sci.,* **61,** 1521–1538.

——, S. K. Krueger, D. Gregory, J.-L. Redelsperger, and W.-K. Tao, 1997: GEWEX Cloud System Study (GCSS) Working Group 4: Precipitating convective cloud systems. *Bull. Amer. Meteor. Soc.,* **78,** 831–845.

Randall, D., M. Khairoutdinov, A. Arakawa, and W. Grabowski, 2003a: Breaking the cloud-parameterization deadlock. *Bull. Amer. Meteor. Soc.,* **84,** 1547–1564.

——, and Coauthors, 2003b: Confronting models with data: The GEWEX Cloud Systems Study. *Bull. Amer. Meteor. Soc.,* **84,** 455–469.

Rotunno, R., W. C. Skamarock, and C. Snyder, 1998: Effects of surface drag on fronts within numerically simulated baroclinic waves. *J. Atmos. Sci.,* **55,** 2119–2129.

Smolarkiewicz, P. K., and L. G. Margolin, 1997: On forward-in-time differencing for fluids: An Eulerian/semi-Lagrangian nonhydrostatic model for stratified flows. *Atmos.–Ocean,* **35,** 127–152.

——, and ——, 1998: MPDATA: A finite-difference solver for geophysical flows. *J. Comput. Phys.,* **140,** 459–480.

——, ——, and A. Wyszogrodzki, 2001: A class of nonhydrostatic global models. *J. Atmos. Sci.,* **58,** 349–364.

Tompkins, A. M., 2001: Organization of tropical convection in low vertical wind shears: The role of water vapor. *J. Atmos. Sci.,* **58,** 529–545.

Werne, J., 1993: Structure of hard-turbulent convection in two dimensions: Numerical evidence. *Phys. Rev.,* **48E,** 1020–1035.

Wu, X., and M. W. Moncrieff, 1996: Collective effects of organized convection and their approximation in general circulation models. *J. Atmos. Sci.,* **53,** 1477–1495.

——, and ——, 2001: Long-term behavior of cloud systems in TOGA COARE and their interactions with radiative and surface processes. Part III: Effects on the energy budget and SST. *J. Atmos. Sci.,* **58,** 1155–1168.

——, W. W. Grabowski, and M. W. Moncrieff, 1998: Long-term behavior of cloud systems in TOGA COARE and their interactions with radiative and surface processes. Part I: Two-dimensional modeling study. *J. Atmos. Sci.,* **55,** 2693–2714.

——, W. D. Hall, W. W. Grabowski, M. W. Moncrieff, W. D. Collins, and J. T. Kiehl, 1999: Long-term behavior of cloud systems in TOGA COARE and their interactions with radiative and surface processes. Part II: Effects of cloud microphysics on cloud–radiation interaction. *J. Atmos. Sci.,* **56,** 3177–3195.

Xie, S.-C., and Coauthors, 2002: Intercomparison and evaluation of cumulus parameterizations under summertime midlatitude continental conditions. *Quart. J. Roy. Meteor. Soc.,* **128,** 1095–1135.

Xu, K.-M., and Coauthors, 2002: An intercomparison of cloud-resolving models with the ARM summer 1997 IOP data. *Quart. J. Roy. Meteor. Soc.,* **128,** 593–624.